CSIRO PUBLISHING

Publications of the Astronomical Society of Australia, 2012, **29**, 309–317
http://dx.doi.org/10.1071/AS11051

Feature Detection in Radio Astronomy using the Circle Hough Transform

C. Hollitt[A,C] *and M. Johnston-Hollitt*[B]

[A]School of Engineering and Computer Science, Victoria University of Wellington, PO Box 600, Wellington 6140, New Zealand
[B]School of Chemical and Physical Sciences, Victoria University of Wellington, PO Box 600, Wellington 6140, New Zealand
[C]Corresponding author. Email: chollitt@ieee.org

Abstract: While automatic detection of point sources in astronomical images has experienced a great degree of success, less effort has been directed towards the detection of extended and low-surface-brightness features. At present, existing telescopes still rely on human expertise to reduce the raw data to usable images and then to analyse the images for non-pointlike objects. However, the next generation of radio telescopes will generate unprecedented volumes of data making manual data reduction and object extraction infeasible. Without developing new methods of automatic detection for extended and diffuse objects such as supernova remnants, bent-tailed galaxies, radio relics and halos, a wealth of scientifically important results will not be uncovered. In this paper we explore the response of the Circle Hough Transform to a representative sample of different extended circular or arc-like astronomical objects. We also examine the response of the Circle Hough Transform to input images containing noise alone and inputs including point sources.

Keywords: radio continuum: general — techniques: image processing

Received 2011 September 15, accepted 2012 January 12, published online 2012 March 13

1 Introduction

The radio sky is rich in scientifically important objects containing circular or arc-like structures. These objects range in physical size from the shells of dying stars to shocks created in merging clusters of galaxies. On the small scale, objects such as supernova remnants stereotypically contain complete or partial circular shells, or in cases when their symmetry is distorted, both (Mineshige & Shibata 1990). Arc-like features are also found in Active Galactic Nuclei (AGN), either in the overall source shape as in the case of bent-tail radio galaxies (Johnston-Hollitt et al. 2004; Mao et al. 2009), or as features observed within the lobes of the AGN themselves (Feain et al. 2011). Finally, giant Mpc-scaled radio relics, which occur on the edges of merging clusters, are found as single or double arc-like regions (Johnston-Hollitt 2003; Bonafede et al. 2009). In addition to their arc-like morphology, these objects are often low in surface brightness and exhibit breaks or gaps which make them hard to detect in an automated fashion. This is particularly true of techniques that rely on either high signal-to-noise or continuous edges in order to define the full extent of the source.

In order to reliably detect broken, low-surface-brightness sources we require algorithms which do not rely solely on the behaviour of individual pixels, but exploit additional non-local information. The advantages of such algorithms are that they are robust in the presence of non-connectedness and noise. Examples of such techniques include template matching, wavelet and related integral transforms and Hough transforms. As the Hough transform is known to be robust to the presence of partial or occluded target objects and to noise (Davies 1988), it is a natural choice to explore for the automatic detection of circular features in astronomical data.

There has been some previous use of the Hough transform in astronomy. It has been used to remove contamination from optical surveys (Storkey et al. 2004), to characterise echelle orders (Ballester 1994, 1996), and to characterise craters on the moon (Jahn 1994). However, it has not been previously applied for either source detection or characterisation in radio astronomy. The increased resolution and field of view that will become routine when using instruments like the Square Kilometre Array (SKA) (Schilizzi, Dewdney & Lazio 2008) and its precursors such as the Australian SKA Pathfinder (ASKAP) and the Murchison Widefield Array (MWA), force a paradigm shift towards greater reliance on automated data extraction techniques such as that described here.

In this work we concentrate on the detection problem, that of locating circular regions of radio emission that are unlikely to have arisen from statistical fluctuations in image noise. We also believe that the techniques described in this paper could contribute to the related characterisation problem, where morphological features of the uncovered emission are accurately determined.

As a result in this paper we have concentrated on detecting circular structures, rather than the accuracy or precision with which they are described.

In this paper we present a description of the circle Hough transform (CHT) in Section 2, followed by a detailed discussion of the applications of the CHT as a detection algorithm for use in Radio Astronomy in Section 3. Section 4 presents a discussion of computational issues and response to image artifacts and presents a suggested framework for the practical implementation of the CHT for next generation radio telescopes. We present a summary of the work and final conclusions in Section 5. We have adopted a standard set of cosmological parameters throughout with $H_0 = 73\,\mathrm{km\,s^{-1}\,Mpc^{-1}}$, $\Omega_\mathrm{m} = 0.27$ and $\Omega_\Lambda = 0.73$.

2 Circle Hough Transforms

The family of algorithms known collectively as Hough transforms are capable of finding and characterising a variety of geometrical objects in image or image like-data (Duda & Hart 1972; Kerbyson & Atherton 1995). The application of the Hough transform for circle detection was a very early development in the field, and has since found wide application (Kimme, Ballard & Sklansky 1975; Illingworth & Kittler 1988; Rad, Faez & Qaragozlou 2003).

In its simplest form the circle Hough transform is computationally challenging, with both computational effort and memory consumption scaling as $O(n^3)$ when transforming an $n \times n$ pixel image. Many variants of the CHT algorithms have consequently been developed to improve the computational performance of the algorithm (Davies 1988; Kerbyson & Atherton 1995; Ioannou, Huda & Laine 1999; Chiu, Lin & Liaw 2010), but current implementations of the CHT remain confined mostly to offline processing.

As is the case for all Hough transforms, the CHT seeks to map an image into a quantised parameter space that describes the target objects. An arbitrary circle in two dimensions can be described by

$$(x - x_0)^2 + (y - y_0)^2 - r^2 = 0, \qquad (1)$$

where x_0 and y_0 are the x and y coordinates of the centre of the circle and r is the circle's radius. Each different three-tuple $\mathbf{x} := (x_0,\ y_0,\ r)$ uniquely parametrises different circles that may be present in an image. Each point in the Hough space therefore corresponds to a complete circle with a particular location and size. The operation of the CHT is to map the input image into the parameter space such that the transform has a high value for parameter tuples consistent with objects that are present in the image.

In its common form, the Hough transform operates on each image pixel independently. For each pixel the algorithm finds the set of parameter tuples that would result in an object passing through the considered pixel. That is, consideration of an image pixel $f(x_i, y_i)$ finds the set $\mathcal{P}$ of all (x_0, y_0, r) tuples that satisfy Equation 1;

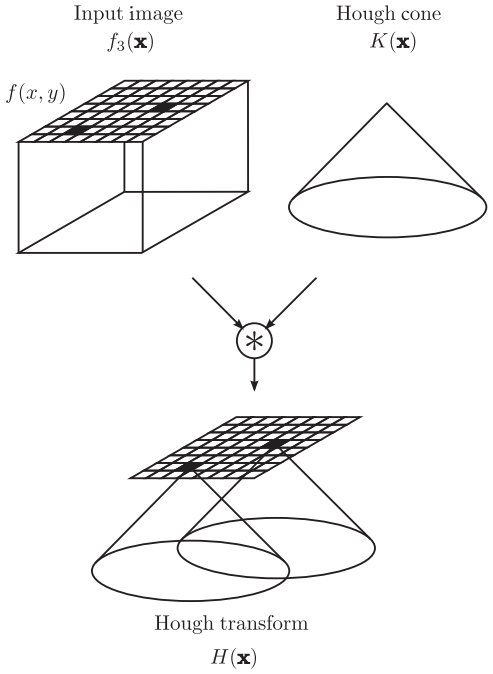

Figure 1 Formation of the Hough transform via convolution. The input image $f(x,y)$ is extended to three dimensions and then convolved with the vote distribution $K(\mathbf{x})$ to generate the Hough transform $H(\mathbf{x})$. For clarity we have represented the Hough cone as smooth, though it is discretised on the same scale as the input image.

$$\mathcal{P} = \{(x_0, y_0, r) : (x_i - x_0)^2 + (y_i - y_0)^2 - r^2 = 0\} \qquad (2)$$

Each location in Hough space that corresponds to a member of $\mathcal{P}$ is then incremented. Thus each image pixel can be regarded as casting a set of 'votes', for those parameter tuples that are consistent with itself. Examination of Equation 2 reveals that the set of votes arising from a single pixel forms a right cone in Hough space (Duda & Hart 1972; Yuen et al. 1990).

The vote distributions from multiple image pixels are added and produces a high number of votes for parameter combinations that describe geometric figures that are actually present in the image. The operation of the CHT can be conveniently regarded as the three-dimensional convolution of the input image with the conical vote distribution (Hollitt 2009), as illustrated in Figure 1.

For our application, if we calculate the CHT of a radio image and then find the peak in the Hough transform we will recover the radius and center of any circular astronomical features in the input radio map.

2.1 Detection Procedure

Peaks in the Hough transform of an arbitrary input image can arise even in the absence of a circular region of diffuse emission. In this section we briefly discuss the production of peaks due to noise in the input image and note that peaks are also expected because of the presence of point sources.

Let us first consider the expected Hough peak size that would arise in Hough space as a result of input

https://doi.org/10.1071/AS11051 Published online by Cambridge University Press

image amplitude noise, which we expect to be normally distributed with mean $\hat{a}$ and standard deviation s, i.e. the input image is $\sim\mathcal{N}(\hat{a}, s^2)$. When searching for a circle having radius r the Hough transform adds the magnitudes of approximately $2\pi r$ pixels. For a random input image we would therefore expect that the distribution of magnitudes for the Hough transform would be $\sim\mathcal{N}(2\pi r\hat{a}, 2\pi r s^2)$.

One can therefore select an appropriate threshold for the source detector as $2\pi r\hat{a} + \zeta s(2\pi r)^{1/2}$, for ζ the number of standard deviations above the expected mean that one wishes to use. For an image a few hundred pixels in extent, $\zeta = 5$ should ensure that Hough peaks arising solely from noise are rarely encountered. A considerably more aggressive threshold could be used if a higher false-positive detection rate were acceptable for a particular application.

The noise in radio images arising from surveys is unlikely to be stationary, so the appropriate values of $\hat{a}$ and s will need to be calculated locally (Huynh et al. 2012). Note also that the analysis above would need to change slightly if the Hough transform were used to search for structures in polarimetric surveys, as the noise in polarisation images is Rician rather than Gaussian.

We would also expect that the Hough transform of an arbitrary radio image will contain a number of putative circles due to the presence of point sources. In a noiseless image the Hough transform would find circles centered half way between each pair of point sources. Such circles will have a diameter approximately equal to the separation of the points sources. However in a noisy image the circle is typically slightly displaced to include high noise pixels in its circumference, as well as the two point sources.

A circle can also be fitted though any set of three points (with the exception of three collinear points), so we would also expect that the Hough transform of an arbitrary field would contain a peak corresponding to each combinations of three point sources. However, in practice many such peaks would correspond to very large circles, or circles with centres lying well outside the image boundaries. That is, if the image contains N point sources then the Hough space will include $\binom{N}{3}$ peaks. In the case of perfect point sources, the magnitude of these peaks would be the sum of the amplitudes of the three selected sources. In practice they will deviate somewhat from this due to the non-ideal beam pattern.

As the magnitudes of the Hough peaks arising from point sources are dependent on the source intensities, it is impossible to remove their effects with a simple threshold. Instead it will be necessary to examine circles detected with the Hough transform to determine whether they have arisen via this mechanism. We have not yet examined this problem in detail, though it will be an important component of any system intended to automatically process survey data using the Hough transform.

Combinations of more point sources are of course also possible if they happen to lie on a common circle, though this becomes increasingly unlikely as the number of points increases.

The overall procedure proposed to find peaks in Hough space is as follows.

1. Find the peak Hough transform amplitude for each value of r.
2. Calculate how many standard deviations above the expected noise-only level $2\pi r\hat{a}$ the maximum value of the Hough transform lies for each r.
3. Search for local maxima in the resulting amplitude as r varies. Such local maxima correspond to circles in the input image.
4. Check for circles that obtain most of their votes from two (or more) point sources and remove them from the list of possible diffuse emission candidates.

An example of this procedure is provided in Section 3.2.

3 Results

We applied the CHT to images containing a variety of arc-like radio sources in order to test features of the algorithm including filtering and robustness in the presence of noise. The variant of the CHT used is described in Hollitt (2009), though the results described below are not dependent on the particular implementation of the algorithm. Each of the three species of source tested — SNRs, tailed radio galaxies and giant radio relics — represent populations which will be present in next generation radio surveys. It is expected that important science will be determined from the statistical characterisation of such populations, making reliable automatic classification an important goal.

3.1 Response to Non-Diffuse Structures

We expect that the distribution of the Hough transform of a Gaussian noise field $\sim\mathcal{N}(\hat{a}, s^2)$ will be centered on $2\pi r\hat{a}$ with standard deviation $s(2\pi r)^{1/2}$. This allows us to determine an appropriate threshold to assess the reliability of any proposed circle detections.

Gaussian noise fields of 243×243 pixels were prepared with the pixels values distributed with known mean and variance. The Hough transform was then calculated to find the distribution of the magnitudes in Hough space. For each value of r the largest value in the Hough transform was found and compared with the theoretical distribution.

Figure 2 shows the results of one such simulation, having the input pixels distributed as $\sim\mathcal{N}(1, 0.25)$. As can be seen the largest values for the Hough transforms typically lie between three and four standard deviations from the expected value of the transform. This is consistent with the expected extreme value of 243^2 samples drawn from a normal distribution.

We therefore conclude that for the image size of 243^2 pixels used throughout this paper, a threshold of five times the input image standard deviation is sufficient to exclude features in Hough space arising from image noise.

https://doi.org/10.1071/AS11051 Published online by Cambridge University Press

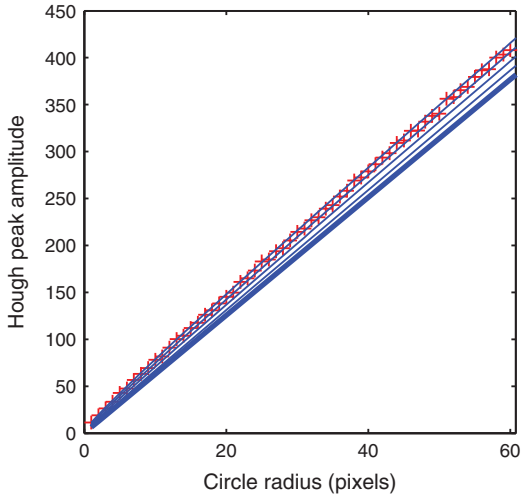

Figure 2 The red crosses indicate the largest value of the Hough transform, taken across the 243^2 values for each target circle radius. The bold blue line indicates the expected value for the Hough transform of the random input field, with the thinner lines indicating progressive steps of one standard deviation in the expected value of the Hough transform.

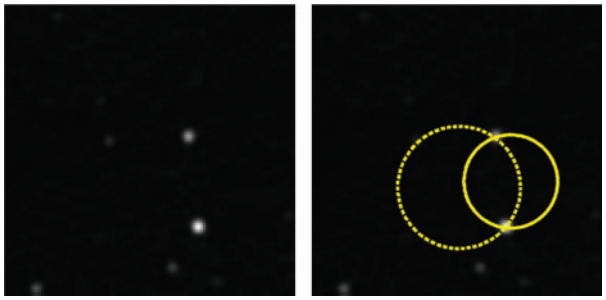

Figure 3 Response of the Circle Hough Transform to a collection of point sources. The centre of the solid circle lies between the two bright point sources. The dashed circle also passes through a third point source to the left of the image.

Figure 3 shows the result of applying the Circle Hough Transform to an image from the Molonglo Galactic Plane Survey (MGPS, Green et al. 1999) containing no known diffuse structures, but a number of isolated point sources. As discussed in Section 2.1, the Hough transform results in a peak corresponding to a circle centered roughly between the two brightest point sources. It also finds a second circle that additionally passes through a third point source.

3.2 Supernova Remnants

When a massive star at the end of its life becomes a supernova, an energetic shock wave is released from its surface. As the shock travels outward it accelerates electrons in the interstellar medium to produce emission at radio frequencies. In the simplest case the resulting emission would be spherically symmetric as the spherical shock passes through a homogeneous interstellar medium. However, where the shock wave is asymmetric, or when there is exiting structure in the gas cloud surrounding the supernova, then more complicated supernova remnants are produced (Gaensler & Slane 2006; Orlando et al. 2007).

Our galaxy contains a large number of known supernova remnants (SNRs), the result of supernovæ occurring in roughly the last million years. The Molonglo Observatory Synthesis Telescope Supernova Remnant Catalogue (MSC) (Whiteoak & Green 1996) contains a list of 75 SNRs from the 843 MHz survey of the Southern Galactic plane within the area $245 \leq l \leq 355°$ in Galactic longitude and $b = \pm 1.5°$ from the Galactic plane. Statistical studies of the SNR population allows much more information to be inferred than would be possible by examination of one SNR alone. In addition to the valuable information gleaned on the average nature of the ISM surrounding supernovæ, statistical analysis shows that there is presently a significant discrepancy between the total number of known SNRs and that expected from stellar lifecycles (Brogan et al. 2006). Comparison with the expected rate of supernovæ production from OB star counts, pulsar creation rates, iron abundance and observation of supernova in other galaxies suggests that there should be over 1000 SNRs detectable in the Galactic plane (Li et al. 1991; Tammann et al. 1994). However, at present only ~250 have been found despite an increasing number of surveys of the region (Green 2004; Brogan et al. 2006). The detection of the population of SNRs is therefore an important aspect of radio surveys of the Galactic disk.

The missing SNRs are believed to be those that are young and distant and those which are old and nearby (Green 2004; Brogan et al. 2006). In the former case the issue is simply a lack of resolution in current surveys of the Galactic plane leading to such small angular sized, bright sources being misclassified as point sources. This issue will be readily addressed and resolved by the next generation of radio telescopes such as the SKA. In the latter case however, the SNRs will be both faint and large and if the present manual 'eyeballing' techniques continue to be used (Whiteoak & Green 1996; Filipović et al. 2002; Brogan et al. 2006) they are likely to remain elusive. Additionally, manual inspection is error prone and often results in objects being missed in the initial data release (Whiteoak & Green 1996; Green 2004). Finally, while this approach has been adequate (although not ideal) in the past, future generations of radio telescopes will generate such a vast stream of data that manual inspection will not be practical.

We have selected a subset of four representative supernova remnants from the MCS catalogue, as shown in Figure 4. This subset was selected to range from a near complete ring (4a), through two partial rings (4b and 4c) to a distorted example (4d). These four SNRs were intended to provide an increasing challenge for the algorithm.

A CHT algorithm was performed on each of the four supernova remnants using the procedure outlined in (Hollitt 2009). The four input data sets were each padded to 243 pixels square. A Hough transform calculation is

https://doi.org/10.1071/AS11051 Published online by Cambridge University Press

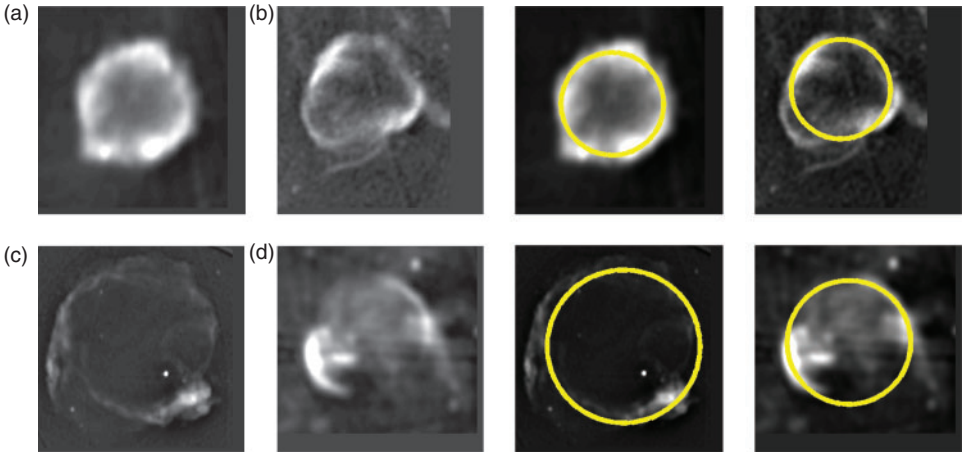

Figure 4 Four supernova remnants taken from the MCS catalogue (Whiteoak & Green 1996). On the left panel subfigure (a) is G337.3+1.0, (b) is G302.3+0.7, (c) is G315.4–2.3 and (d) is G317.3–0.2. On the right panel are the same four objects overlaid with circles that indicate the features detected via the Hough Transform of each object.

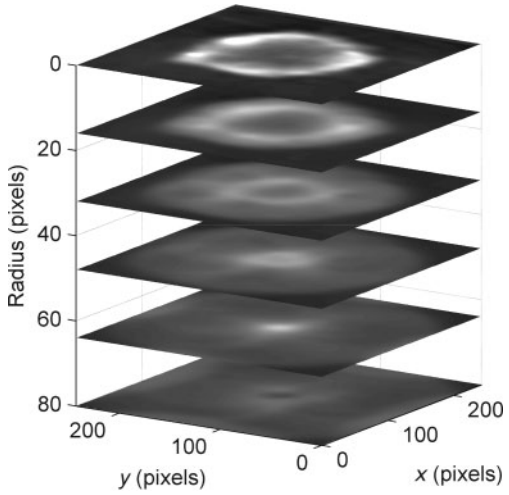

Figure 5 Slices through the Hough transform of G337.3+1.0. Slices are taken through several planes corresponding to a set of different possible SNR radii, $r = (16, 32, 48, 64, 80)$ pixels.

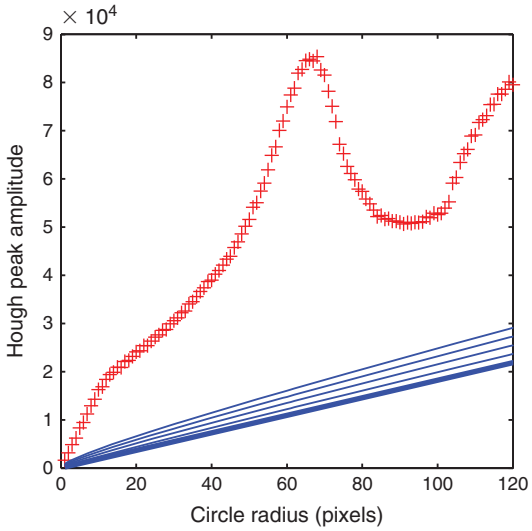

Figure 6 Maximum values of the Hough transform of G337.3+1.0 as a function of radius are indicated by the red crosses. The thick lower line indicates the Hough transform expected from the image noise alone, with the increasingly higher lines indicating one standard deviation in the expected noise-only values.

typically preceded by an edge detection step to highlight the boundaries of objects. However, supernova remnants are inherently shell-like, so we found the edge-detection step to be unnecessary. Comparison of the transformation of the raw and edge-detected data resulted in differences in only a few pixels in the estimated SNR position and radius.

Figure 5 shows the Hough transform of one of the SNRs. For clarity we selected the almost complete ring of G337.3+1.0. While the Hough transform results in a full three-dimensional array this is difficult to present graphically. The figure therefore shows the magnitude of the Hough transform obtained for a small subset of the possible SNR radii. As can be seen for small radii the intensity pattern is well distributed, indicating that there is no strong peak for these radii and hence no small radius circles in the image. However, in the $r = 64$ plane we can see a strong peak toward the centre of the field. This indicates that the input image contains a circle with radius approximately 64, which is located toward the centre of the image. For larger radii we again see the intensity pattern is spread, so there are no larger circles present.

The Hough transforms of the four SNRs were searched to find their maxima. As an example of the procedure used, Figure 6 shows the peak value of the Hough transform of G337.3+1.0 as a function of the target circle radius. Also shown in the figure are the peak values expected if the image contained noise alone. The figure clearly shows that the input image contains features other than noise.

The height of the peak above the noise-only level is then calculated in units of standard deviations, that is, we calculate the statistical significance of the Hough

https://doi.org/10.1071/AS11051 Published online by Cambridge University Press

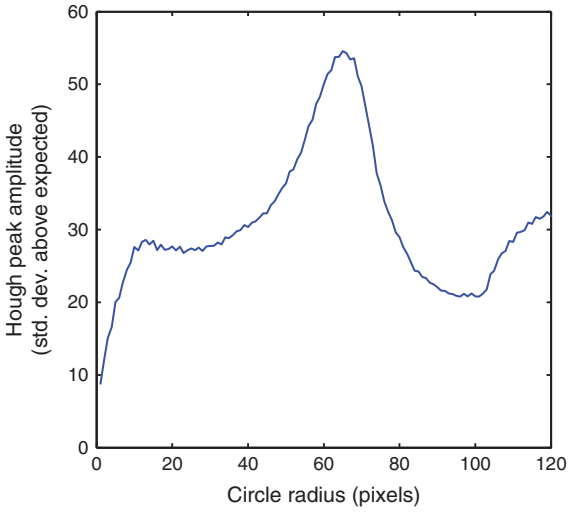

Figure 7 Maximum value of the Hough transform of G337.3+1.0 as a function of radius. The amplitude is expressed as the number of standard deviations between the peak value and the value expected from a field consisting solely of Gaussian noise.

transform. The result of this calculation is shown in Figure 7. Local maxima in this graph indicate peaks in Hough space, which can then be used to extract the location of circles in the original image. In the case of Figure 7, the prominent peak at a radius of 65 pixels corresponds to the shell of the supernova remnant. The local maxima around 10 pixels is associated with the circular feature in the lower right portion of the SNR, as seen in Figure 4a.

These peaks in the transforms correspond to the circle that is most consistent with the input data in each case. Extraction of the coordinates of the peaks therefore results in an estimate of the location and radius of the supernova remnants. The effectiveness of the CHT in identifying the circular structures in the four supernova remnants can be seen in Figure 4. In all four cases the best fitting circles returned by the algorithm are in good agreement with the radio data.

3.3 Bent-Tail Radio Galaxies

Bent-tail (BT) galaxies are Fanaroff–Riley class I/II (Fanaroff & Riley 1974) radio sources that consist of a core, coincident with the optical host galaxy, and two tails of bent radio emission. The bending of the radio jets is believed to result from the actions of ram pressure (Gunn & Gott 1972) due to the relative motion of the galaxy and its surrounding. In the classic case this results in a 'C'-shaped radio object such as SUMSS J032752–532613 (Johnston-Hollitt et al. 2004) seen on the left of Figure 8, though more complicated structures such as PKS J0327–532 seen on the right of the same figure do occur.

BTs have been found in the densest and most turbulent regions of galaxy clusters in the local ($z < 0.07$) Universe (Mao et al. 2009) at a rate of about 1–2 per cluster. BTs are thought to act as signposts for over-densities in large-scale structure, with associations between tailed-galaxies and clusters persisting out to at least $z \sim 2$ (Dehghan et al. 2011; Dehghan et al., in preparation) making them an important class of objects for science with future all-sky radio survey.

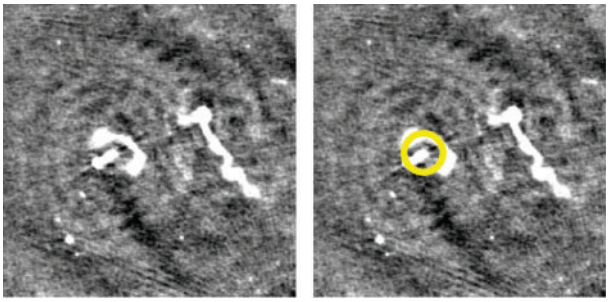

Figure 8 1.4 GHz image of a pair of head-tailed radio galaxies located in the centre of Abell 3125 (Johnston-Hollitt et al. 2004). The classic 'C' shaped HT (SUMSS J032752–532613) has been correctly identified by the CHT over all of the other radio sources and artifacts in the image.

One of the most important parameters to extract when using BT galaxies to obtain physical information on the environment in which they are embedded is the radius of curvature of the source (Freeland, Cardoso & Wilcots 2008; Free-land 2010). This technique is only applied to wide-angle tailed sources (WAT) such as SUMSS J032752–532613, so it is typically performed subsequently to the initial source detection phase. For the test described in this section we wished only to find the radius of the WAT, rather than extract information about the many wiggles in the tails of the other BT. Consequently we imposed a constraint on the allowable circle radii before running the transform. This demonstrates the ability of the CHT to search for sources of only a certain angular size and to perform the simultaneous science-driven detection and charactisation of the WATs. The successful results are seen in the left of Figure 8.

As discussed in more detail in Section 4.2, radio telescopes with only a few elements suffer from gaps in the *uv*-plane which result in circular artifacts in the image-plane. In the case of the image used here, the image, from Johnston-Hollitt et al. (2004), comprises of a mosaic of 4 pointings of 1.4-GHz data from 1.5- and 6-km configurations of the pre-CABB Australia Telescope Compact Array (ATCA) which is known to have significant gaps in the distribution of baseline lengths. The size of the resultant artifacts in the image plane is a function of the antenna element spacing and is therefore known in advance allowing us to employ filtering to prevent the CHT returning artifacts as sources. As next generation radio telescopes will employ a larger number of elements, this is likely not to be a major issue for future surveys.

3.4 Radio Relics

Radio relics are a rare class of large arc-like radio sources seen on the periphery of galaxy clusters. They are believed to be the result of shockwaves which occur when clusters of galaxies merge, the most powerful events since

https://doi.org/10.1071/AS11051 Published online by Cambridge University Press

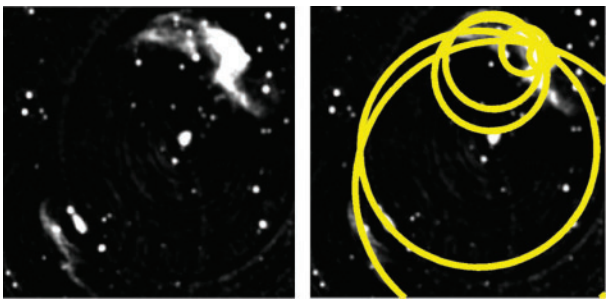

Figure 9 1.4 GHz Australia Telescope Compact Array (ATCA) mosaic image of the double relic cluster Abell 3667 (Johnston-Hollitt 2003), this image covers approximately four square degrees on the sky and shows an example of one of the largest arc-like sources known. The CHT has identified the arc-like shape of the northern relic as well as bifurcations in the intensity structure of the source.

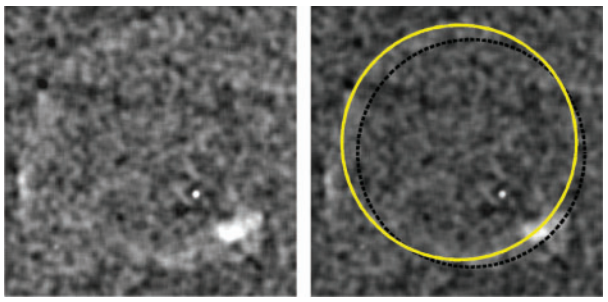

Figure 10 The input and results when the noise level in the supernova remnant from Figure 4c is increased until the Hough transform method is 50% reliable. The solid line indicates the location of the SNR as estimated by the Hough transform. The dashed circle indicates the location of the SNR as predicted without additional noise added to the image before processing.

the Big Bang. The physical size of these sources can be up to six million light year across, such as in the northern relic in Abell 3667 seen in Figure 9. Because of their extremely low surface brightness they are very difficult to detect with conventional pixel threshold based searches. As in the case of faint SNRs, radio relics should be more easily detected with algorithms utilising non-local information such as the CHT.

We tested the CHT on the field of Abell 3667 using 1.4-GHz ATCA data from Johnston-Hollitt (2003). These data use five different configurations of the telescope and so have good sampling of the *uv*-plane and hence a minimum of circular artifacts. This particular image has had a taper applied in the *uv*-plane to give a resolution of approximately one arcminute. The data contain a number of extended sources including the double relics for A3667 that are located to the top right and bottom left of the image, two BT galaxies in the centre of the field and at the lower left above the relic and a number of unresolved point sources. The CHT was employed without the filtering described in Section 3.3 and the resultant detected features in Hough space are displayed on the right side of Figure 9.

Use of the CHT should isolate the location and scale of all circular features in a set of radio data to provide a catalogue of possible sources that can be assessed by an astronomer. In this case the algorithm correctly identifies the curvature of the northern relic and gives the approximate cluster centre (largest circle). It also correctly characterises an internal curved structure in this relic (smallest circle). However, the characterisation of the relics is imperfect as Abell 3667 has an elliptical, rather than perfectly circular structure. Also the middle circle is influenced by the bright BT galaxy just north of the cluster centre which is unrelated to the relic.

3.5 Robustness to Noise

To illustrate the robustness of the CHT to noise we contaminated the supernova remnants in Figure 4 with increasing amounts of Gaussian noise and processed the resulting images until the SNRs could no longer reliably be detected.

Figure 10 shows the supernova in Figure 4c contaminated with additional noise until the Hough transform detector was 50% reliable. For this object the magnitude of the noise has been increased by a factor of 10 from that in the original image. As shown in the figure, the estimated location of the SNR in the contaminated image is slightly different to that in the uncontaminated image. However, as we are primarily interested in the detection of supernova remnants rather than their characterisation, we do not regard this as a significant problem. As might be expected the error in the suggested location of the object typically decreases as the signal-to-noise ratio of the images improves.

4 Discussion

4.1 Computational Issues

Unfortunately the CHT is a computationally intensive algorithm, particularly when used to characterise circles with unconstrained radii (Yuen et al. 1990). The CHT is therefore likely to prove too slow to directly process the vast amounts of raw data that will be produced by the next generation of radio telescopes such as the SKA.

Instead, we propose a two tiered approach to the detection of circular and arc-like sources. The first stage will require the detection of regions of extended radio emission (that is emission from any objects other than point sources). This initial processing must be fast, but doesn't need to be very accurate. Some variety of blob-detection algorithms would be suitable for this purpose. A fair amount of work has been carried out by the astronomical community on this problem and standard algorithms such as VSAD (Condon et al. 1998) and DUCHAMP (Whiting 2012) exist. Ideally the blob detection algorithm would additionally provide an estimate of the scale of a possible source. However, existing astronomical application of blob detection are poor at detecting broken large scale structures, so are likely to provide a poor estimate of both the size and centre of most SNRs or double relics.

https://doi.org/10.1071/AS11051 Published online by Cambridge University Press

4.2 Artifacts

Existing telescopes currently operating with $\nu \leq 3$ GHz necessarily use a relatively sparse sampling of spatial frequencies, which can result in circular calibration artifacts in their output data. Such artifacts would confound our detection algorithm in its simplest incarnation. However, as demonstrated in Section 3.3, grating lobes of known size can be filtered out before the final catalogue is returned. Additionally, many artifacts have circular features combined with radial spikes, allowing a combined CHT and linear Hough transform to be used to find and reject such sources. This would have the additional benefit of being able to identify flawed regions in an automatically generated image before a survey was released.

5 Conclusions

We have examined the Circle Hough Transform as a detection and characterisation method for finding circular or arc-like sources in astronomical data. We have tested the algorithm on MGPS and ATCA images of a range of sources including supernova remnants, tailed radio galaxies and radio relics which all represent scientifically important classes of radio sources for the next generation of radio telescopes. We have shown that the technique is successful at recovering such sources and providing physical information for them in an automated way.

At present thresholding algorithms such as DUCHAMP (Whiting 2012) are able to produce catalogues of radio sources based on the requirement of having a certain number of contiguous pixels over a certain signal-to-noise level. These algorithms will usually return either the position of the brightest pixel or the geometrical centre of the source as the central coordinate. This approach will work adequately for the majority of symmetrical, unbroken sources. However, for arc-like sources such techniques will not produce the correct coordinates making automatic cross-matching to other wavelengths difficult (as is currently the case). Additionally, with broken sources such as SNRs and double relics, such techniques will report multiple, unrelated diffuse sources (all with the wrong central coordinates) rather than identify a single source.

Because it uses non-local information, the CHT is able to work with broken sources and is capable of detecting sources that have much lower signal-to-noise ratios than other algorithms. The CHT can therefore be expected to do a superior job of both detecting and characterising some classes of sources, particularly those that are very diffuse.

However, as the CHT is computationally expensive, it is unlikely to be sensible to run the algorithm over the entire sky for an all-sky survey such as EMU (Norris et al. 2011). We propose that it would be better to use a conventional 'blob detection algorithm' to preprocess the data before and then apply the CHT in certain parts of the sky only. These regions could either be selected based on criteria from the results of the conventional blob detection, or as regions where such low-surface-brightness, arc-like sources are expected such as in the Galactic plane or around galaxy clusters. This tiered approach is likely to be the most efficient method for generating a robust catalogue of diffuse radio sources and will be the subject of further experimentation.

There are several improvements that could be made to the current CHT. Firstly, the robustness of the method can be improved by the development of a more effective method for searching the Hough transform for peaks. Simply finding the maximum value as we have done here is unlikely to be the optimal technique. Secondly, as seen in some SNRs and double relics, the objects in question are elliptical rather than circular. The Hough transform could be extended from the current circular implementation to an elliptical version. However this increases the number of parameters required and hence would result in a five dimensional Hough space which would considerably increase the computation complexity.

As has been noted, the Circle Hough Transform produces apparent circles as a result of point sources. If the Hough transform is to prove effective at automatic diffuse source detection, it will need to be combined with additional processing to remove the effects of point sources. Once this has been done the effectiveness of the combines detection system can be assessed by using it on a catalogue containing known diffuse structures.

A catalogue of known supernova remnants has been manually compiled from the second Molonglo Galactic Plane Survey (MGPS2) (Murphy et al. 2007), allowing ready comparison with the results of the automatic detection. Use of the CHT on such a dataset will allow the determination of the false negative and false-positive detection of the technique. This comparison also admits the possibility of the detection of as-yet undiscovered supernova remnants and in particular those in the class of being old and faint which have been predicted via several independent indicators but remain, as yet, undetected. Thus, in addition to characterising the false-positive and false-negative error rates, performing the CHT on the MGPS2 could address one of the current problems in understanding the so-called 'Galactic Ecology'.

Acknowledgment

The MOST is operated by The University of Sydney with support from the Australian Research Council and the Science Foundation for Physics within The University of Sydney. The Australia Telescope is funded by the Commonwealth of Australia for operation as a National Facility managed by CSIRO.

References

Ballester, P., 1994, ASPC, 61, 319
Ballester, P., 1996, VA, 40, 479
Bonafede, A., Giovannini, G., Feretti, L., Govoni, F. & Murgia, M., 2009, A&A, 494, 429
Brogan, C. L., Gelfand, J. D., Gaensler, B. M., Kassim, N. E. & Lazio, T. J. W., 2006, ApJL, 639, 25

https://doi.org/10.1071/AS11051 Published online by Cambridge University Press

Chiu, S. H., Lin, K. H. & Liaw, J. J., 2010, International Journal of Pattern Recognition and Artificial Intelligence, 24, 457
Condon, J. J., Cotton, W. D., Greisen, E. W., Yin, Q. F., Perley, R. A., Taylor, G. B. & Broderick, J. J., 1998, AJ, 115, 1693
Davies, E. R., 1988, PaRe, 7, 37
Dehghan, S., Johnston-Hollitt, M., Mao, M., Norris, R. P., Miller, N. A. & Huynh, M., 2011, JApA, 32, 491
Duda, R. O. & Hart, P. E., 1972, Commun. ACM, 15, 11
Fanaroff, B. L. & Riley, J. M., 1974, MNRAS, 167, 31
Feain, I., et al., 2011, ApJ, 740, 17
Filipović, M. D., Stupar, M., Jones, P. A. & White, G. L., 2002, ASPC, 271, 387
Freeland, E., 2010, ASPC, 423, 93
Freeland, E., Cardoso, R. F. & Wilcots, E., 2008, ApJ, 685, 858
Gaensler, B. M. & Slane, P. O., 2006, ARA&A, 44, 17
Green, D. A., 2004, BASI, 32, 335
Green, A. J., Cram, L. E., Large, M. I. & Ye, T., 1999, ApJS, 122, 207
Gunn, J. E. & Gott, J. R., III, 1972, ApJ, 176, 1
Hollitt, C., 2009, in Proc. 24th Int. Conf. Image and Vision Comput. New Zealand (IVCNZ 09), ed. D. Bailey (Wellington: IEEE), 373
Huynh, M., Hopkins, A., Norris, R., Hancock, P., Murphy, T., Jurek, R. & Whiting, M., 2012, PASA, Special Issue on Source Finding and Visualization
Illingworth, J. & Kittler, J., 1988, CVGIP, 44, 87
Ioannou, D., Huda, W. & Laine, A. F., 1999, Image and Vision Comput., 17, 15
Jahn, H, 1994, SPIE, 2357, 427
Johnston-Hollitt, M., 2003, PhD Thesis, Univ. Adelaide
Johnston-Hollitt, M., Fleenor, M., Rose, J., Christiansen, W. & Hunstead, R. W., 2004, IAUC, 195, 423
Kerbyson, D. J. & Atherton, T. J., 1995, in 5th Int. Conf. on Image Processing and its Applications (Edinburgh: IEEE), 370
Kimme, C., Ballard, D. & Sklansky, J., 1975, Commun. ACM, 18, 120
Li, Z., Wheeler, J. C., Bash, F. N. & Jefferys, W. H., 1991, ApJ, 378, 93
Mao, M. Y., Johnston-Hollitt, M., Stevens, J. B. & Wotherspoon, S. J., 2009, MNRAS, 392, 1070
Mineshige, S. & Shibata, K., 1990, ApJL, 355, 47
Murphy, T., Mauch, T., Green, A., Hunstead, R. W., Piestrzynska, B., Kels, A. P. & Sztajer, P., 2007, MNRAS, 382, 382
Norris, R. P., et al., 2011, PASA, 28, 215
Orlando, S., Bocchino, F., Reale, F., Peres, G. & Petruk, O., 2007, A&A, 470, 927
Rad, A. A., Faez, K. & Qaragozlou, N., 2003, in VIIth Digital Image Computing: Techniques and Applications, ed. C. Sun, H. Talbot, S. Ourselin & T. Adriaansen (Melbourne: CSIRO), 879
Schilizzi, R. T., Dewdney, P. E. F. & Lazio, T. J. W., 2008, SPIE, 7012, 52
Storkey, A. J., Hambly, N. C., Williams, C. K. I. & Mann, R. G., 2004, MNRAS, 347, 36
Tammann, G. A., Loeffler, W. & Schroeder, A., 1994, ApJS, 92, 487
Whiteoak, J. B. Z. & Green, A. J., 1996, A&AS, 118, 329
Whiting, M. T., 2012, MNRAS, in press (astroph/1201.2710)
Yuen, H. K., Princen, J., Illingworth, J. & Kittler, J., 1990, Image and Vision Comput., 8, 71

https://doi.org/10.1071/AS11051 Published online by Cambridge University Press